Experimental Approach to Interaction Physics Challenges of the Shock Ignition Scheme Using Short Pulse Lasers

C. Goyon,[1] S. Depierreux,[1] V. Yahia,[2] G. Loisel,[2] C. Baccou,[2] C. Courvoisier,[1] N. G. Borisenko,[3] A. Orekhov,[3] O. Rosmej,[4] and C. Labaune[2]

[1]*CEA, DAM, DIF, F-91297 Arpajon, France*

[2]*LULI, Ecole Polytechnique, CNRS, CEA, UPMC, 91128 Palaiseau, France*

[3]*P. N. Lebedev Physical Institute, Russian Academy of Sciences, 119991 Moscow, Russia*

[4]*GSI Helmhotzzentrum fur Schwerionenforschung, 64291 Darmstadt, Germany*

(Received 26 April 2013; revised manuscript received 17 July 2013; published 5 December 2013)

An experimental program was designed to study the most important issues of laser-plasma interaction physics in the context of the shock ignition scheme. In the new experiments presented in this Letter, a combination of kilojoule and short laser pulses was used to study the laser-plasma coupling at high laser intensities for a large range of electron densities and plasma profiles. We find that the backscatter is dominated by stimulated Brillouin scattering with stimulated Raman scattering staying at a limited level. This is in agreement with past experiments using long pulses but laser intensities limited to 2×10^{15} W/cm^2, or short pulses with intensities up to 5×10^{16} W/cm^2 as well as with 2D particle-in-cell simulations.

DOI: 10.1103/PhysRevLett.111.235006 PACS numbers: 52.38.Bv, 52.38.Dx, 52.50.Jm

The shock ignition scheme opens the possibility to reach ignition in laser fusion with a reduced laser energy compared to previous schemes, direct and indirect drives [1]. In this scheme, a strong shock is launched at the end of the compression phase by adding a short (a few hundreds of picoseconds) high-intensity pulse that ignites the compressed fuel leading to a high fusion gain [2]. However, the numerical simulations predicting ignition are obtained with untested assumptions on the laser-plasma coupling efficiency which is not so well known in this regime [3]. While the plasma conditions, electron density, and temperature are the same as those encountered by the compression laser pulse, the shock ignition pulse is more intense by at least 1 order of magnitude. This means that all the nonlinear processes, plasma instabilities [4,5] which were possibly under control for the compression phase, may grow in an uncontrolled way, dramatically reducing the coupling of this pulse with the plasma and, consequently, the strength of the shock. The strategy that is needed to mitigate the risks associated with the shock pulse propagation and coupling needs a good understanding of the physics of the different processes.

Among the different plasma instabilities, stimulated Brillouin (SBS) and Raman (SRS) scattering, two-plasmon decay and filamentation are the most dangerous processes. Although significant progress has been achieved in numerical simulations of laser-plasma coupling, those are not yet predictive for large plasmas and high-intensity conditions. The linear gain analysis indicates that, under the shock ignition interaction conditions, the convective amplification of SBS should be very significant and that SRS should be strong in front of the quarter critical density leading to dramatic losses of energy [6]. However, calculated SBS reflectivities have been successful only if nonlinear processes do not play an important role [7]. Filamentation of the beam may result in beam spraying, reducing the energy in the vicinity of the critical density as well as modifying the interaction conditions and consequently the growth of SBS and SRS. It is impossible to predict numerically what will result from the mutual interplay between these three instabilities as many nonlinear effects, including coupling between the plasma waves, secondary decays, or kinetic effects may occur. Above all, both SBS and SRS can be in particular regimes for the shock ignition (SI) interaction conditions, the strongly coupled regime for SBS [8] and the inflationary regime for SRS [9], for which there is almost no experimental data. Experimentally, it is difficult to obtain both a large hot plasma and high laser intensity. Most experiments to date have focused on moderate intensity, below 3×10^{15} W/cm^2 and long pulses [10,11]. But to achieve the required pressure (~ 300 Mbar) to ignite the core, the shock spike must have higher intensities ($\sim 5 \times 10^{15} - 3 \times 10^{16}$ W/cm^2). Past experiments have measured SBS reflectivities with laser intensities higher than 5×10^{15} W/cm^2 and pulse duration between 1 and 150 ps [12–15]. Some of them have shown high SBS reflectivities, up to 43%. However, the temperature and size of the preformed plasma were limited by the amount of available energy of the laser beams and there was no control of the laser intensity distribution. In terms of plasma parameters of interest, typically, at the arrival time of the shock pulse, the plasma corona will have an extent of around 1 mm with a characteristic density scale length $L_n \sim 300$–700 μm, and an electron temperature $T_e \sim 2$–3 keV [16].

We have designed dedicated experiments, associating long, high energy, and short, high-intensity, laser pulses

to study the propagation and the energy deposition of a high-intensity laser pulse in a preformed long and hot plasma under well-controlled interaction conditions. For the first time, the short, high-intensity pulse was focused through a random phase plate leading to a well-defined intensity distribution in the focal volume. The primary contribution of this work is to bring new experimental results on laser-plasma coupling in a regime that has never been explored before. Our results show that the backscatter is dominated by stimulated Brillouin scattering with stimulated Raman scattering staying at a limited level. Filamentation has been observed but does not seem to play a significant role on the laser-coupling. The message of this manuscript is that the SBS loss of energy is a potentially serious handicap for the SI scheme and it is needed to find a way to control it.

Experiments have been carried out on the Pico2000 laser facility at the LULI laboratory. This facility couples two laser beams, one in the nanosecond regime, and one in the picosecond regime, in the same vacuum chamber. The setup is shown in Fig. 1(a), with the two beams at 112.5° from each other. The long pulse delivers 400 J in 1.5 ns, square pulse, at 0.53 μm of laser light. It was focused with an $f/4$ lens through random phase plates with elongated elements producing an elliptical focal spot of 100×500 μm^2 or 100 μm $\times$ 1 mm full width at half maximum (FWHM) and an average intensity of $2–5 \times 10^{14}$ W/cm^2. It was used to preform a plasma from either a thin-exploded foil or a low-density foam [17]. Strips of CH foils with initial thickness of 1.5, 2.5, and 3.5 μm and 500 μm–1 mm width and foams of 3, 6, 10, and 12 mg/cc with 500 μm–1 mm length were used to produce quasihomogeneous plasmas of different initial electron density. The short laser pulse was sent along this direction, delivering 20 J in 5 ps at 0.53 μm. It was focused with an $f/4$ off-axis parabola through a random phase plate leading to a 100 μm diameter (FWHM) focal spot composed of speckles with a well-known intensity distribution in vacuum, shown in Fig. 2(a), and average intensities between 2×10^{15} and 3×10^{16} W/cm^2. The time delay between the two beams was 1.5 ns, so the short laser pulse interacted with a millimeter-long plasma having a well-defined electron density and a temperature in the keV range without cross-beam effects. For some shots, a stack of foam of increasing densities was used to create a density profile rising up to the critical density, completing the data in inhomogeneous plasmas. As shown in Fig. 1(b) in the case of a stack of foam with initial densities of 3, 6, and 12 mg/cc with 300 μm length each, it was possible to generate a plasma profile close to the one of the corona of a compressed target. Diagnostics mainly focused on the powers and spectra of the scattered light collected in the backward direction of the short pulse laser for both the Raman and Brillouin spectral ranges and on the transmitted light through the plasma with 2D and 1D far field images. In backscatter, the light was collected in the incident aperture and analyzed with two combinations of spectrometer-streak camera with a spectral resolution of 1 and 50 Å for the SBS and SRS stations, respectively. In transmission, the light was collected in twice the incident aperture. The streak cameras were needed to separate the contributions from the long and the short pulses. All diagnostics were absolutely calibrated *in situ* with laser shots of known energy.

In the first part of the experiment, shots were dedicated to the plasma characterization, electron density, and temperature. For the thin exploded foils, the electron density was deduced from the Raman spectra at low interaction intensity which exhibited a narrow component. Using the

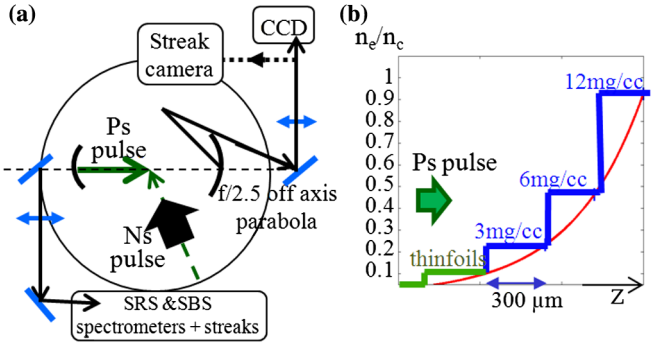

FIG. 1 (color online). (a) Setup of the experiment showing the two laser beams with long, high energy and short, high-intensity pulses, and the main diagnostics. (b) Schematic view of the density profiles along the interaction laser axis of a composed foam target (blue steps) and of the shock ignition corona (red curve) as calculated in numerical simulations [16].

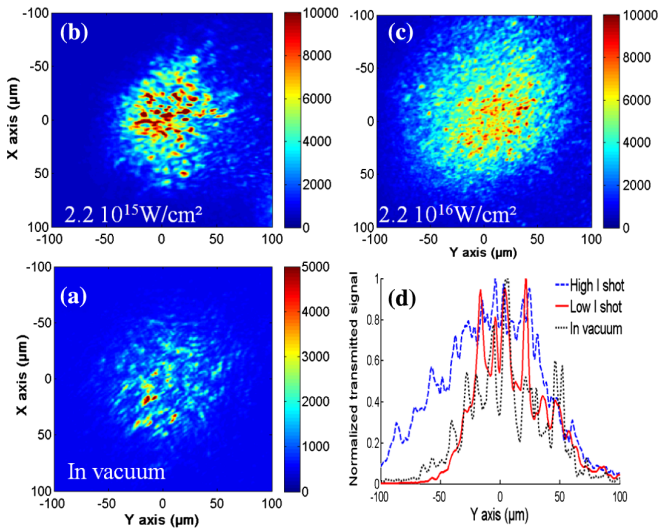

FIG. 2 (color online). 2D far-field images of the intensity distribution of the picosecond laser. (a) In vacuum, (b) inside the plasma produced from a 10 mg/cc foam with 500 μm length at 2×10^{15} W/cm^2, and (c) at 2×10^{16} W/cm^2. (d) Outline along the y direction of the 2D distribution for these two intensities.

standard relationship between the Raman wavelength and the plasma density [4,5], the densities were 0.05, 0.11, and 0.21 ($\pm$ 0.02) times the critical density ($n_c = 4 \times 10^{21}$ cm^{-3}) at the top of the profile for the foils with initial thickness of 1.5, 2.5, and 3.5 μm, respectively. For the low-density foam, the velocity of the ionization front produced by the nanosecond pulse alone was measured by imaging the sidescattered 2ω on a streak camera looking at the output plane of the plasma. This has enabled us to control the penetration depth of the nanosecond pulse in the plasma and so to precisely adjust the picosecond beam axis position to study its propagation and coupling in fully ionized foam plasma having an electron density given by the initial density of the foam. For 3, 6, 10, and 12 mg/cc, the electron densities were [0.22, 0.44, 0.8, and 0.91 ($\pm$ 0.05)] n_c. The electron temperature was $T_e \sim (0.9 \pm 0.15)$ keV; it was measured using characteristic transitions in H- and He-like Cl ions doped for diagnostic purposes into the foam samples. Time-integrated spectra have been measured by means of a focusing spectrometer with spatial resolution using a spherically bent mica crystal as a dispersive element and an image plate as a detector.

For all the explored conditions, laser intensities, from 2×10^{15}–3×10^{16} W/cm^2, and all plasma densities, the maximum SRS reflectivity stayed below 7%. A diagnostic was set to look for emission at 1.06 μm, the half harmonic of the incident laser wavelength, which is a signature of processes occurring near the quarter critical density layer, two-plasmon decay (TPD) and absolute Raman, but no signal was observed within the limit of the sensitivity of the detector, demonstrating a conversion efficiency below 10^{-3} of the initial laser energy. From these experimental results, it seems that neither SRS, nor TPD are a problem as far as losses of energy or for the production of suprathermal electrons for these conditions.

Evidence of plasma smoothing were observed from the 2D images of the intensity distribution at the output of the plasma. As expected, the effects were stronger at high plasma density. In Figs. 2(b) and 2(c), the intensity distributions at the output of the plasma are shown for the case of a 10 mg/cc foam for two laser intensities, 2.2×10^{15} and 2.2×10^{16} W/cm^2. At low laser intensity, the intensity distribution is similar to that observed in vacuum [Fig. 2(a)], showing that it was not modified by the propagation of the laser pulse in the plasma. On the other hand, at high laser intensity there is some widening of the initial focal spot diameter by ~40% (FWHM) compared to the low intensity case and a clear smoothing of the spikes. Traces along a diameter, shown in Fig. 2(d), demonstrate a reduction by a factor of 4 of the contrast at high intensity. This transition is observed within parameters, plasma density and laser intensity, in agreement with the usual criterion based on the ratio between the average speckle power and the critical power [18] showing that the plasma induced beam smoothing was produced by collective forward stimulated Brillouin scattering and filamentation. However, the total amount of light outside the aperture beam was less than 20% of the transmitted light, so we concluded that filamentation was not relevant for determining the laser coupling.

SBS was studied as a function of the interaction intensity and plasma density in quasihomogeneous plasmas of 500 μm length as well as in increasing density profiles up to the critical density. A typical time-resolved spectrum of the backscattered SBS light from a $0.11 n_c$ plasma at maximum intensity is shown in Fig. 3(a). The first signal in time corresponds to scattered light from the nanosecond beam at 112.5°. The second signal is the backward SBS spectrum of the picosecond pulse. Its height corresponds to the width of the streak camera slit. The spectrum of the picosecond pulse in vacuum is shown in the bottom part of Fig. 3(a) for reference. SBS spectra have been recorded for various electron densities at high interaction intensity and they are shown in Fig. 3(b). For low initial electron density

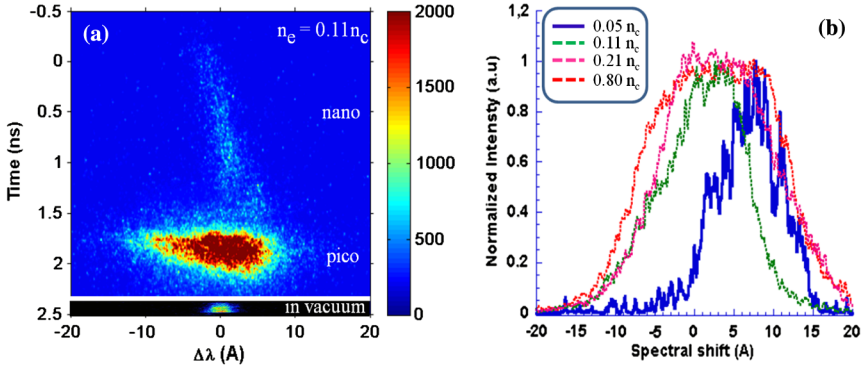

FIG. 3 (color online). (a) Time-resolved spectrum of the light collected in the focusing optics of the picosecond beam showing, as a function of time, the scattered light from the nanosecond pulse and the backscattered SBS light from the picosecond pulse with an intensity of 2.5×10^{16} W/cm^2; the spectrum of the picosecond pulse in vacuum is shown in the bottom part of the image with a reduced temporal scale. (b) SBS spectra of the picosecond pulse at maximum intensity for preformed plasmas of various initial maximum densities.

($0.05n_c$), the width of the SBS spectrum is almost twice that of the picosecond pulse, and is redshifted by 7–8 Å. This shift corresponds to the expected SBS shift (given by the ion-acoustic frequency) for an electron temperature of $\sim(0.8 \pm 0.15)$ keV [4,5]. For higher electron densities ($> 0.1n_c$), we observe a broadening of the spectra to the blue, the largest broadening being obtained for the highest initial density (10 mg/cc foam). Part of this broadening could be explained by an extension of the SBS activity in areas where the plasma expansion toward the laser produces a blue Doppler shift that is superimposed on the SBS shift. This had been observed previously in a similar plasma-beam configuration using Thomson scattering from the ion-acoustic waves (IAW) associated with SBS [19]. Moreover, at high intensity and high electron density, SBS is in the strongly coupled regime [8] as its growth rate is $\gamma_{\mathrm{SBS}} = 2.95 \times 10^{-3}\ \omega_0[\mathrm{I}_{14}\lambda_0^2 n_e/n_c(n_c - n_e)/n_c]^{1/3} \sim 0.56 \times 10^{-2}\omega_0 \sim 4\omega_{\mathrm{iaw}}$, where ω_0 is the laser frequency, so is larger than the ion acoustic frequency ω_{iaw}. In this regime the IAW spectrum is rather broad and the amplification gain is not too sensitive to the frequency mismatch, which could explain the observed spectra.

The broadening of the spectra is accompanied by a strong increase of the SBS reflectivity. The evolution of the SBS reflectivity as a function of the plasma density at high laser intensity and as a function of the laser intensity for the high-density plasmas are shown in Figs. 4(a) and 4(b), respectively. Very high levels $(\sim 60 \pm 5)\%$ of SBS reflectivity are observed for densities close to critical and intensity of 2.5×10^{16} W/cm^2. Shots with compound targets, (3 + 6) mg/cc, and (3 + 6 + 12) mg/cc, produced similar reflectivities as the 6 or the 10 mg/cc foams with similar length, showing that the important parameter is the maximum electron density of the preformed plasma. The dependency of the SBS reflectivity as a function of the laser intensity displays a continuous increase of the reflectivities with the intensity with no evidence of saturation. This is different from previous results with short pulses of Refs. [14,15] that displayed reflectivities below 10% up to intensity $\sim 10^{17}$ W/cm^2. The difference may be attributed to the plasma density effect as these former SBS measurements were obtained in low-density plasmas, below $0.05n_c$, and these new experiments demonstrate that this is a critical parameter.

Numerical simulations have been performed for parameters close to those of this experiment. The 2D simulations with relativistic particle-in-cell code predict that SBS dominates the coupling for times longer than $\sim 7000\omega_0^{-1} \sim 2$ ps [20,21], which is shorter than our pulse duration. They find a reflectivity of $\sim 5\%$ for an intensity of 4×10^{16} W/cm^2 and a maximum electron density of $0.4n_c$. This is close to our measurements, which provide reflectivities of 1% to 10% for electron density varying from $0.2n_c$ to $0.4n_c$. From the comparison between the experimental and the numerical results, it seems that kinetics effects and the interplay between filamentation or cavitation, which destroys the coherency of the resonant coupling, is dominating the SBS growth. The temporal resolution of the experimental diagnostics cannot capture all the fine features of Raman, but our results confirm that, even if Raman is in the inflationary regime, the reflectivities stay at a low level. The absence of a TPD signature in the experiment is in agreement with the fact that it is observed to saturate very quickly in the simulations.

The two main questions are then how to extrapolate the SBS results to higher plasma temperature and to times longer than our pulse duration at high intensity. At high temperature, one can expect low collisional absorption in the low density part of the profile and consequently more laser energy arriving in the high density part. From our results, this will produce an increased SBS reflectivity. The mechanisms described just after, leading to SBS saturation, will also be less efficient at high temperature. For longer pulse duration, one can expect that filamentation, self-focusing, and stimulated forward Brillouin scattering will produce smoothing of the laser intensity distribution as observed in the experiment. This results in speckles of smaller diameter than the initial ones, which are stable

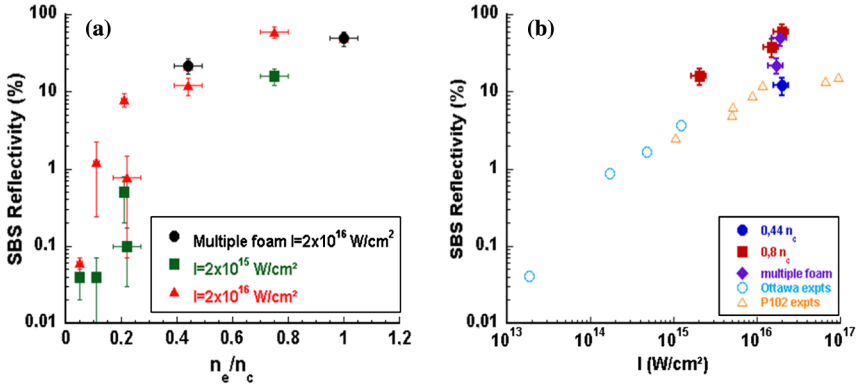

FIG. 4 (color online). (a) SBS reflectivity as a function of the maximum plasma electron density for two interaction intensities. (b) SBS reflectivity as a function of the picosecond pulse intensity for various plasma densities; former results (open symbols) from experiments with short pulse lasers, Ottawa [14] and P102 [15], are plotted on the same graph for comparison.

for SBS. This can lead to SBS saturation at lower levels than what is measured in 5 ps. The nonlinear evolution of SBS was studied in the limit of a fluid description with the harmonic decomposition method [22]. Fluid-type nonlinearities of the ion acoustic waves (IAW) associated with SBS can reduce its growth due to SBS-induced flow modification and/or due to IAW harmonics generation. These simulations show that IAW harmonics generation can transform the coherent three-wave SBS coupling into an incoherent type that leads to a first phase of large and bursty SBS reflectivity followed by reduction or suppression of SBS at long time due to nonlinear ion wave effects. The parameters of our experiments correspond to this first phase and large levels of IAW harmonics were observed in the simulations. Longer pulse duration experiments display reflectivities close to 40% [10,11,23]. This does not take into account the scattered light outside the focusing optics that can significantly increase these values.

In conclusion, plasma instabilities have been studied in long (mm) and hot (keV) preformed plasmas at high laser intensity. The main result is that SBS dominates the laser-plasma coupling for all conditions explored in this work. This is in agreement with multidimensional kinetic simulations and demonstrates that the laser-plasma coupling efficiency is a serious issue for the success of the SI scheme unless a good control of SBS is found.

The authors gratefully acknowledge stimulating discussions with D. Pesme, V. T. Tikhonchuk, P. E. Masson-Laborde, C. Riconda, P. Loiseau, S. Hüller, M. Casanova, and W. Rozmus. We also thank the LULI 2000 operating team for its participation in this experiment and the support of the ANR CORPARIN contract.

[1] J. D. Lindl, *Inertial Confinement Fusion* (Springer, New York, 1998); S. Atzeni and J. Meyer-ter-Vehn, *The Physics of Inertial Fusion* (Oxford University Press, Oxford, 2004); J. D. Lindl, R. I. McCrory, and E. M. Campbell, Phys. Today **45**, No. 9, 32 (1992).

[2] R. Betti, C. D. Zhou, K. S. Anderson, L. J. Perkins, W. Theobald, and A. A. Solodov, Phys. Rev. Lett. **98**, 155001 (2007); V. A. Shcherbakov, Sov. J. Plasma Phys. **9**, 240 (1983); L. J. Perkins, R. Betti, K. N. LaFortune, and W. H. Williams, Phys. Rev. Lett. **103**, 045004 (2009); A. J. Schmitt, J. W. Bates, S. P. Obenschain, S. T. Zalesak, and D. E. Fyfe, Phys. Plasmas **17**, 042701 (2010); B. Canaud and M. Temporal, New J. Phys. **12**, 043037 (2010); S. Yu. Gus'kov, Plasma Phys. Rep. **39**, 1 (2013).

[3] M. Lafon, X. Ribeyre, and G. Schurtz, Phys. Plasmas **20**, 022708 (2013).

[4] W. L. Kruer, *The Physics of Laser Plasma Interaction* (Addison-Wesley, New-York, 1998).

[5] D. Pesme *et al.*, *Interaction Collisionnelle et Collective*, La Fusion Thermonucléaire par Laser Vol. 1, edited by R. Dautray and J. P. Watteau (Eyrolles, Paris 1993).

[6] O. Klimo, V. T. Tikhonchuk, X. Ribeyre, G. Schurtz, C. Riconda, S. Weber, and J. Limpouch, Phys. Plasmas **18**, 082709 (2011).

[7] S. H. Glenzer *et al.*, Nat. Phys. **3**, 716 (2007).

[8] A. A. Andreev, C. Riconda, V. T. Tikhonchuk, and S. Weber, Phys. Plasmas **13**, 053110 (2006).

[9] H. X. Vu, D. F. DuBois, and B. Bezzerides, Phys. Plasmas **9**, 1745 (2002); I. N. Ellis, D. J. Strozzi, B. J. Winjum, F. S. Tsung, T. Grismayer, W. B. Mori, J. E. Fahlen, and E. A. Williams, Phys. Plasmas **19**, 112704 (2012).

[10] S. Depierreux *et al.*, Plasma Phys. Controlled Fusion **53**, 124034 (2011).

[11] W. Theobald *et al.*, Phys. Plasmas **19**, 102706 (2012).

[12] L. M. Goldman, J. Soures, and M. J. Lubin, Phys. Rev. Lett. **31**, 1184 (1973); B. H. Ripin, F. C. Young, J. A. Stamper, C. M. Armstrong, R. Decoste, E. A. McLean, and S. E. Bodner, Phys. Rev. Lett. **39**, 611 (1977).

[13] D. W. Phillion, W. L. Kruer, and V. C. Rupert, Phys. Rev. Lett. **39**, 1529 (1977); R. Turner and L. M. Goldman, Phys. Rev. Lett. **44**, 400 (1980); K. A. Tanaka and L. M. Goldman, Phys. Rev. Lett. **45**, 1558 (1980).

[14] H. A. Baldis, D. M. Villeneuve, B. La Fontaine, G. D. Enright, C. Labaune, S. Baton, Ph. Mounaix, D. Pesme, M. Casanova, and W. Rozmus, Phys. Fluids B **5**, 3319 (1993).

[15] S. D. Baton, C. Rousseaux, Ph. Mounaix, C. Labaune, B. La Fontaine, D. Pesme, N. Renard, S. Gary, M. Louis-Jacquet, and H. A. Baldis, Phys. Rev. E **49**, R3602 (1994).

[16] X. Ribeyre, G. Schurtz, M. Lafon, S. Galera, and S. Weber, Plasma Phys. Controlled Fusion **51**, 015013 (2009).

[17] N. G. Borisenko *et al.*, J. Phys. Conf. Ser. **112**, 022013 (2008); J. Limpouch *et al.*, Plasma Phys. Controlled Fusion **46**, 1831 (2004).

[18] H. Rose and D. Dubois, Phys. Fluids B **5**, 590 (1993); M. Grech, G. Riazuelo, D. Pesme, S. Weber, and V. T. Tikhonchuk, Phys. Rev. Lett. **102**, 155001 (2009).

[19] C. Labaune, H. A. Baldis, E. Schifano, B. Bauer, A. Michard, N. Renard, W. Seka, J. D. Moody, and K. G. Estabrook, Phys. Rev. Lett. **76**, 3727 (1996).

[20] C. Riconda, S. Weber, V. T. Tikhonchuk, J.-C. Adam, and A. Heron, Phys. Plasmas **13**, 083103 (2006).

[21] C. Riconda, S. Weber, V. T. Tikhonchuk, and A. Heron, Phys. Plasmas **18**, 092701 (2011).

[22] S. Huller, P. E. Masson-Laborde, D. Pesme, M. Casanova, F. Detering, and A. Maximov, Phys. Plasmas **13**, 022703 (2006).

[23] S. Depierreux *et al.*, Phys. Rev. Lett. **102**, 195005 (2009); S. Depierreux, P. Loiseau, D. T. Michel, V. Tassin, C. Stenz, P.-E. Masson-Laborde, C. Goyon, V. Yahia, and C. Labaune, Phys. Plasmas **19**, 012705 (2012).